New Generation Layered Nanocomposites Derived from Ethylene-*co*-Vinyl Acetate and Naturally Occurring Graphite

Jinu Jacob George,[1] Abhijit Bandyopadhyay,[2] Anil K. Bhowmick[1]

[1]*Rubber Technology Centre, Indian Institute of Technology, Kharagpur 721302, India*
[2]*Department of Polymer Science and Technology, University of Calcutta, Kolkata 700009, India*

Received 4 May 2006; accepted 3 July 2006
DOI 10.1002/app.25067
Published online 28 January 2008 in Wiley InterScience (www.interscience.wiley.com).

ABSTRACT: New ethylene-*co*-vinyl acetate (EVA, with 60% vinyl acetate content) based nanocomposites were prepared with graphites modified by various techniques and a commercially available expanded graphite (EG). The infrared spectra and the surface energy measurements indicated better oxidation and higher surface energy of the graphite modified by mixed acids followed by high temperature treatment (GO). Interlayer space and surface area were increased as a result. EG possessed higher surface area. GO was found to distribute in finer tactoids of average thickness of 25 nm in the matrix, as compared with the unmodified graphite (UG), having average tactoid thickness more than 40 nm along with aggregation. EG also showed finer dispersion in the EVA matrix with some network formation. The dynamic mechanical and the mechanical properties were superior at the 2 wt % concentration of the GO, beyond which the improvement was less, possibly because of aggregation of GO. Greater EVA-GO interaction at 2 wt % concentration was also supported from the swelling analysis, thermal conductivity, and the thermo-oxidative degradation data of the hybrid composites. The melt viscosity was lower at 2 wt % GO concentration. EG based nanocomposites registered similar properties. © 2008 Wiley Periodicals, Inc. J Appl Polym Sci 108: 1603–1616, 2008

Key words: graphite; nanocomposite; reinforcement

INTRODUCTION

Since the introduction of polyamide 6/clay hybrid nanocomposites via intercalation polymerization, the research and application on this area has made a striking progress till date. The ever-increasing interest in nanoscience and technology using fillers of nano dimensions in polymer matrices are principally due to some exceptional properties that are derived from the resultant materials.[1–4] These nano fillers could be spherical metal oxides,[5–7] nanotubes,[8,9] or layered clays.[10–13]

Till date, numerous literatures have been published from various laboratories including ours, exploring the different aspects of clay[14–19] and silica[20–24] based polymer nanocomposites. Clay is the first generation layered, one-dimensional nanofiller, whereas silica is the spherical, zero-dimensional nano filler among the metal oxide family. In the last five years, layered graphite has appeared in the arena as new generation one-dimensional nano filler for the polymeric systems with a lot of promise.

Correspondence to: A. K. Bhowmick (anilkb@rtc.iitkgp.ernet.in).

Contract grant sponsor: DRDO, New Delhi, India.

Graphite is an allotrope of carbon, the structure of which consists of graphene layers stacked along the *c*-axis in a staggered array.[25]

It has been known since long back that certain atoms and molecules swell graphite and increase its weight. In the modern terminology, this phenomenon has been elucidated as the intercalation of guest chemical moieties within the graphene layers of the host graphite lattice.[26]

High crystallinity of graphite is disadvantageous in forming the nanocomposites with polymers, as the giant polymer molecules do not find spaces within the graphene sheets. This has been overtaken by modifying the graphite flakes with several oxidizing agents.[27] This treatment introduces some polar groups on to graphite, which helps in widening the interlayer spacing in the material so that giant polymer molecules get access into it. The modified graphite, quite often, has been termed as graphite oxide and designated as GO.[28] The chemical modification turns graphite slightly hydrophilic and therefore better dispersion could be anticipated within polar polymer matrices. Till date, some literatures are available on nonpolar thermoplastics like polystyrene by using *in situ* intercalative polymerization technique[29] along with few polar polymers like polyamide[30] and poly(methyl methacrylate).[26] But the authors are not aware of any reference on graphite

nanosheet composites comprising of thermosetting matrices, especially rubbers. Under this backdrop, the present article explores the synthesis and characterization of novel rubber grade ethylene-*co*-(vinyl acetate) (EVA) (which is a commercially important copolymer of ethylene and vinyl acetate, having various applications[31])–graphite hybrid nanocomposites. The article is segmented in two parts: The first part describes the modification and characterization of naturally occurring graphite powders. Commercially available expanded graphite has also been used for comparison in few instances to gain control over the tailor-made filler material. The second part deals with preparation and characterization of the EVA–graphite hybrid nanocomposites. Structure-property correlation has also been attempted against the experimental findings of these systems. This investigation will have applications in the development of EVA having higher thermal stability, mechanical properties, and thermal conductivity at low loading of graphite.

EXPERIMENTAL

Materials

Rubber grade ethylene vinyl acetate (EVA) with 60% vinyl acetate content was supplied by Bayer (now Lanxess), Germany. Naturally occurring graphite powder (UG) was supplied by Comet Chemicals, Mumbai. The commercial graphite, which is already expanded (EG), was supplied by Asbury Graphite Mills, United States. The oxidizing agents, concentrated sulfuric acid (H_2SO_4), concentrated nitric acid (HNO_3), potassium permanganate ($KMnO_4$), and hydrogen peroxide (H_2O_2) and the crosslinker for the rubber, dicumyl peroxide (DCP, 99% pure), all of laboratory grade were obtained from s.d. Fine-Chemicals, Mumbai, Ranbaxy, S.A.S Nagar, E. Merck (India), Mumbai and Hercules India, respectively. Hexamethylene diamine (HMDA), another agent for the modification of the natural graphite was generously supplied by NICCO, India. Triallyl cyanurate (TAC), the cocrosslinker was procured from Fluka A G, Germany. Toluene of LR grade, used as the solvent for EVA was obtained from MERCK (India), Mumbai, India.

Different methods of modification of naturally occurring graphite flakes

The naturally occurring graphite powder (UG) was modified by the following three different methods:

Mixed acid treatment

UG of 10 g was added to a mixture of concentrated H_2SO_4 (98%) and HNO_3 (72%), taken in the volume ratio of 4:1 in a 250-mL beaker. The mixture was stirred well using a mechanical stirrer for 18–20 h at room temperature (27°C) and then dried in an air oven to remove any moisture present. Afterwards, that was taken in a silica crucible and heat treated at 900°C for 30 s in a muffle furnace to prepare the modified graphite (GO). The method is similar to that reported in the literature.[32]

Potassium permanganate/mixed acid treatment

Graphite powder (5 g) was digested with a mixture of 100 mL of H_2SO_4 (98%) and 16.5 mL of HNO_3 (72%) for 30 min in an ice bath and then 30 g of $KMnO_4$ was added to the mixture and stirred for additional 30 min in a 250 mL RB flask. The temperature was brought to room temperature with constant stirring. The excess $KMnO_4$ was removed by adding H_2O_2 at a very slow rate. Immediately after the addition of H_2O_2, excess distilled water was added and washed for several times. The water present was removed by drying at around 100°C in the air oven. This is similar to the procedure carried out by Gopakumar.[33]

Amine treatment

About 1 g of natural graphite was heated with 10 mL of HMDA (0.076 mol) in a 50 mL test tube, in silicone oil bath at (140 ± 10)°C for 2 h. The resulting graphite was washed using ethyl alcohol followed by distilled water and then drying at 80°C in an air oven.[34]

Preparation of EVA-graphite nanocomposites

The nanocomposites were synthesized by using a solution-mixing technique. EVA (5 g per batch) was dissolved in 50 mL of toluene to make 10% solution of the rubber using a magnetic stirrer in a 250 mL beaker. DCP of 0.05 g as the curing agent and 0.05 g of TAC as the coagent was added to the rubber solution. The solution was thoroughly stirred using a mechanical stirrer. The modified graphite powder, dispersed in toluene was first sonicated for 15 min and subsequently added to the rubber solution while stirring at room temperature (27°C) for 15 min. The final solution was cast over teflon trays and kept for air drying followed by vacuum drying at 50°C till there was practically no weight variation. The dried films were molded in a hot press at 150°C for a cure time of 25 min. The composition details of the nanocomposites are reported in Table I.

Characterization of the unmodified, modified graphite, and EVA-graphite nanocomposites

Fourier transform infrared spectroscopy

Fourier transform infrared (FTIR) (model: NICOLET NEXUS ™) in diffuse reflectance infrared Fourier

TABLE I
Designation and Compositions of the Hybrid Composites

No.	Sample designation	Weight %			
		EVA_{60}	UG	GO	EG
1	EVA_{60}	100	0	0	0
2	EVA_{60} + 1GO	100	0	1	0
3	EVA_{60} + 2GO	100	0	2	0
4	EVA_{60} + 4GO	100	0	4	0
5	EVA_{60} + 1UG	100	1	0	0
6	EVA_{60} + 2UG	100	2	0	0
7	EVA_{60} + 4UG	100	4	0	0
8	EVA_{60} + 1EG	100	0	0	1
9	EVA_{60} + 2EG	100	0	0	2
10	EVA_{60} + 4EG	100	0	0	4

transform (DRIFT) mode was employed to characterize the UG and GO powders, whereas EVA-graphite hybrid composite (EVA + GO, EVA + EG, and EVA+ UG, Table I) was analyzed by using the attenuated total internal reflection (ATR) technique with the help of a 450 KRS5 prism. All the spectra were taken within the range of 4000–400 cm^{-1} with the resolution of 4 cm^{-1}. The analysis was done using the software OMNIC E.S.P 5.1.

Particle size analysis

The particle size and surface area of the different graphite samples were measured using a Malvern-3601 (UK) particle size analyzer.

X-ray diffraction studies

The X-ray diffraction studies were done using a Rigaku CN 2005 X-Ray Diffractometer, model: Miniflex (30 kV, 10 mA) with a Cu target (CuKα radiation with $\lambda = 0.154$ nm) in the range of $2\theta = 10^\circ$–50°. The corresponding *d*-spacing of the powder graphite particles was calculated using the Bragg's Equation.[35]

$$n\lambda = 2d \sin \theta \quad (1)$$

where, λ is the wavelength of X-rays, d is the interplanar distance, and θ is the angle of incidence of the radiation.

The crystallite size within the graphite powders before and after modification was determined from the X-ray diffraction data using the following equation:[35,36]

$$C_s = 0.9\ \lambda\ /B \cos \theta \quad (2)$$

where, C_s is the crystallite size, λ is the wavelength of the incident X-ray beam, B the full width at half maximum (FWHM) of the X-ray diffraction peaks, and θ is the half of the angle 2θ corresponding to the peak.

Surface energy measurements

The surface energy of both unmodified and modified graphite particles was calculated by measuring the contact angle using a dynamic wicking method. The graphite powder was tapped 200 times and packed in the graduated capillary tube (2-mm inner diameter). The tube was placed vertically and was contacted with liquids (water and formamide) in the beaker. The liquids penetrated up in to the column of the powders by the capillary attraction. The height of the penetration was calculated by fitting the data of the weight of the penetrating liquid at regular intervals of time in the following equation:

$$h = \omega/\rho S\varepsilon \quad (3)$$

where ω is the weight of the penetrating liquid, h is the height of liquid penetration, ρ the density of the filler, S the surface area of the powder in the packed column, and ε the porosity of the packed column, calculated by the following equation:

$$\varepsilon = 1\ -\ W_p/hS\rho_p \quad (4)$$

W_p is the weight of the powders tapped in the column.The subscript p indicates penetration of the solvent in the column.

The contact angle of the powder sample was calculated using the Washburn Equation[37]

$$h^2 = 2R_{\text{eff}}\gamma_L \cos\ \theta t/\eta \quad (5)$$

where γ_L is the surface tension of the liquid used, θ is the contact angle of the liquid on the graphite powder, t the equilibrium time taken, η the viscosity of the liquid, and R_{eff} is effective radius of the packed column in the capillary tube.

Finally the surface energy of the graphite sample was calculated by measuring the contact angle with water and formamide using the following equation.

$$\cos\theta = -1 + 2(\gamma_s^d\gamma_1^d)^{1/2}/\gamma_L + 2(\gamma_s^p \cdot \gamma_1^p)^{1/2}/\gamma_L \quad (6)$$

where γ_s^d is the dispersive component of the surface energy of the solid surface and γ_1^d is the dispersive component of the surface energy of the liquid surface, γ_s^p is the polar component of the surface energy of the solid surface and γ_1^p is the same of the liquid surface, and γ_L is the surface tension of the liquid.

Morphological observation

Atomic force microscopy. The morphological analysis of the solution cast and molded samples was done using the Multi Mode Scanning Probe Microscope, model: MMAFMLN with a Nanoscope IIIa controller

supplied by the Digital Instruments (Veeco Metrology Group), Santa Barbara, CA. All the measurements were carried out in air at ambient conditions (27°C) using tapping mode probes with constant amplitude. The scanning was done using 125-μm long single beam etched silicon probe (TESP), square pyramid in shape with a spring constant (k) of 20 N/m and nominal radius of curvature of 10 nm. Images of 1.5 μ × 1.5 μ scan area containing 256 data points were analyzed using a Nanoscope image processing software.

Transmission electron microscopy. The samples for TEM analysis were prepared by ultra-cryomicrotomy using a Leica Ultracut UCT. Freshly sharpened glass knives with cutting edge of 45° were used to get the cryosections of 50–70 nm thickness. Since these samples were elastomeric in nature, the temperature during ultra cryomicrotomy was kept at −50°C (which were well below glass transition temperatures of EVA). The cryosections were collected individually on sucrose solution and directly supported on a copper grid of 300-mesh size. The microscopy was performed using a JEOL JEM- 2010 (Japan) transmission electron microscope, operating at an accelerating voltage of 200 KV.

Dynamic mechanical thermal analysis

Dynamic mechanical thermal characteristics of the composite films (0.4–0.6 mm thick) were evaluated by using a DMTA IV (Rheometric Scientific) under tension mode. All the data were analyzed using RSI Orchestrator application software on an ACER computer attached to the machine. The temperature sweep measurements were made over the range of temperatures from −35 to 20°C. The experiments were carried out at a frequency of 1 Hz at a heating rate of 2°C/min. The storage modulus (E') and the loss tangent (tan δ) data were recorded for all the samples under identical conditions.

Swelling study

The swelling studies of the rubber specimens were carried out in toluene at ambient condition (27°C) for 72 h. Volume fraction of rubber, V_r, was calculated using the following equation:[38]

$$V_r = \frac{[(D - F\ W_i)\rho_r^{-1}]}{[(D - F\ W_i)\rho_r^{-1}] + A_0\rho_s^{-1}} \quad (7)$$

where, V_r is volume fraction of rubber in the swollen gel, D, the deswollen weight of the composites, F is the fraction insoluble; W_i the initial weight of the sample and A_0 is the amount of solvent imbibed. The ρ_r is the density of the rubber, while ρ_s is density of the swelling solvent.

Analysis of mechanical properties

The mechanical properties of the composites were evaluated by a universal testing machine (UTM, Zwick 1445) on dumbell specimens, punched out from the cast films using an ASTM Die C. All the tests were carried out as per ASTM D 412-99 method at (25 ± 2)°C at a crosshead speed of 500 mm/min. The average values of three tests for tensile strength, tensile modulus, and elongation at break are reported for each sample.

Rheological studies

The melt flow properties of the uncrosslinked nanocomposites and the virgin rubber samples were measured by means of a Monsanto Processability Tester (MPT) (barrel radius, 9.53 mm), which is a fully automated capillary viscometer. The entire barrel and the capillary assembly were electrically heated with a microprocessor-based temperature controller. The capillary used had a length to diameter ratio of 30 (length, 30.00 mm; diameter, 1.00 mm). The compound entrance angles of the capillary were 45° and 60°. The apparent shear stress was taken as equal to the true shear stress. The extrusion study was carried out at 110°C and at seven different shear rates (12.3, 24.5, 49, 98.1, 147, 196.2, and 245.2 s^{-1}). The rate of shear variation was achieved by changing the speed of the plunger automatically. The apparent shear stress (τ_{app}), apparent shear rate ($\dot{\gamma}_{app}$), and apparent shear viscosity (η_{app}) were calculated using the following set of equations:

$$\tau_{app} = d_c\Delta P/4l_c \quad (8)$$

$$\dot{\gamma}_{app} = 32Q/\pi d_c^3 \quad (9)$$

$$\eta_{app} = \tau_{app}/\dot{\gamma}_{app} \quad (10)$$

where, ΔP is the pressure drop across the length of the capillary, d_c and l_c are diameter and length of the capillary, respectively, and Q, the volumetric flow rate of the material.

Measurements of thermal conductivity

The thermal conductivity of the nanocomposite samples were measured using the instrument DSC204, NETZSCH Thermal Analyzer of Phoenix, United States. The experiment was conducted in an inert atmosphere of nitrogen and the heating was done at a rate of 10°C/min. Thermal conductivity of the vari-

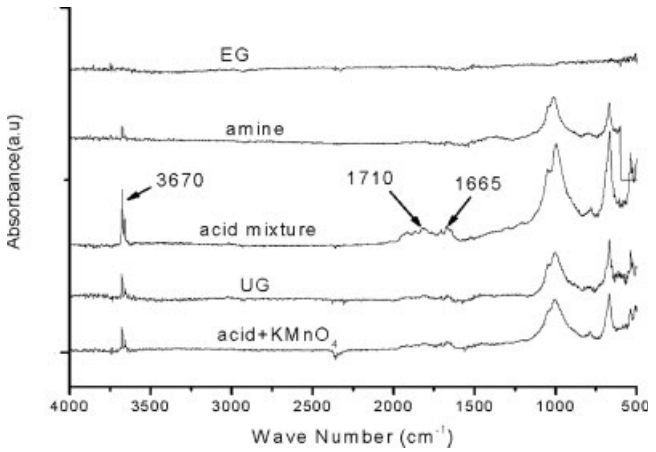

Figure 1 FTIR spectra of naturally occurring unmodified graphite and different modified graphites.

ous samples was calculated using the following equation

$$\text{Heat flow}, Q = -\lambda_1 \, A \, \mathrm{d}T/\mathrm{d}x \qquad (11)$$

where, Q is the heat flow obtained from the DSC curve by taking the amount of heat flow between two temperatures (here 140–165°C). λ_1 is the thermal conductivity expressed in W/m/K/g, A is the sample area (here 3 mm^2), and dx the thickness (here 0.5 mm) of the sample respectively. dT is the temperature difference between the two selected temperatures i.e., $165 - 140 = 25$°C.

Thermal degradation study

Thermal stability of the composites was investigated by thermogravimetric analysis (TGA) by using a Perkin–Elmer TGA instrument [Model: Pyris Diamond TG/DTA] from ambient to 800°C at a programmed heating rate of 20°C/min in oxygen. A sample weight of ~ 10 mg was taken for all the measurements. The weight loss against temperature was recorded. Differential thermo gravimetric analysis (DTG) of the composites was represented in terms of the first derivative plots of the TGA curves. The data points denote the weight loss/time against temperature at the specified heating rate.

RESULTS AND DISCUSSION

Characterization of the filler

Fourier transform infrared spectra and particle size analysis

Figure 1 displays FTIR plots for the unmodified and the modified graphites along with that of the commercially available expanded graphite, by arbitrary stacking. Table II records the actual intensity values (in % absorbance) of important peaks of the unmodified and modified graphites. It is observed both from the stacked figures (Fig. 1) and the table (Table II), C=O absorption band appears at around 1710 cm^{-1} on oxidation with mixed acid and with $KMnO_4$/acid systems (predominant in mixed acid treated system). Apart from this, mixed acid treated sample shows highest peak intensities for the OH (3670 cm^{-1}) and C=C (1665 cm^{-1}) stretching vibrations. Surprisingly, amine treated sample is devoid of these (C=O, OH and C=C) groups. The treatment of the UG with various reagents like mixed acid, $KMnO_4$/ acid, and organic amine is principally aimed at inducing polarity on the graphite surface. Impregnation of several polar functional groups like >C=O and —OH could help in destructuring the crystallites and increase interlayer spacing. This would probably improve the dispersion of the filler within the polymer matrices by predominant intercalation. As demonstrated from the FTIR study, treatment of the UG with mixed acid followed by heat treatment in a muffle furnace produces most effective oxidation (existence of C=O, OH, and C=C groups) as compared with other treatments.

The reaction of UG with mixed acid could be expressed as follows[39]

$$\mathrm{UG} + \mathrm{n}\,\mathrm{H_2SO_4} + n/2[\mathrm{O}] \rightarrow n[\mathrm{UG.H_2SO_4}] + n/2\mathrm{H_2O} \qquad (12)$$

where [O] is the oxidant moiety generated *in situ* from the combination of concentrated H_2SO_4 and HNO_3. The [UG·H_2SO_4] is an intermediate species, which probably undergoes decomposition at high temperature (~ 900°C) to emit gaseous products causing interlayer separation in the graphene sheets.[32] This is specifically termed as graphite oxide (GO), as already mentioned. Here onwards, the mixed acid treated modified graphite sample would only be referred to as GO, unless otherwise mentioned. The FTIR spectra of commercially available expanded graphite contain no peaks indicating that there are no surface groups on the graphite platelets. This may be due to the high temperature treatment of the graphite done in an inert atmosphere. Table III compares the results in the form of average particle size and the specific surface area of different graphite samples

TABLE II
FTIR Peak Intensity of Different Graphite Samples

	Peak intensity (in % absorbance)	
Graphite samples	—OH (3670 cm^{-1})	C=O (1710 cm^{-1})
UG	0.130	–
$KMnO_4/H_2SO_4/HNO_3$ treated	0.132	0.02
Amine treated	0.078	–
H_2SO_4/HNO_3+900°C treated	0.306	0.06
EG	0.058	–

TABLE III
Characteristics of Different Graphite Samples

Graphite sample	Average particle size (μm)	Specific surface area (m^2/cc)	Dispersive component (γ_s^d; mJ/m^2)	Polar component (γ_s^p; mJ/m^2)	Total Surface energy (γ; mJ/m^2)
UG	67.62	0.150	4.41	13.98	18.39
$KMnO_4/H_2SO_4/HNO_3$ treated UG	63.59	0.144	3.66	17.03	20.69
H_2SO_4/HNO_3 + 900°C treated UG	36.64	0.225	0.13	38.68	38.81
EG	21.87	0.320	0.31	14.42	14.73

before and after modification. It is clear that, the treatment with mixed acid (concentrated HNO_3 and H_2SO_4) and on subsequent heating at 900°C in a muffle furnace deagglomerates the graphite sample significantly, more than that with $KMnO_4$/mixed acid treatment at room temperature. In fact, the average particle size of the latter is quite close to that of the unmodified graphite sample (Table III). As the specific surface area is inversely proportional to the average particle size, the mixed acid treatment produces the highest surface area (among the laboratory treated samples) compared with $KMnO_4$/ acid treated sample. The data for the amine treated sample is deliberately being put off the list, as it shows very little amination or oxidation not detected in the FTIR study.

Increase in polarity causing some deagglomeration is further confirmed from the measurements of surface energy through contact angle study. Table III compares these data on UG and GO samples. Because of oxidation, the polar component is increased significantly in the case of GO and as a complementary fact the dispersion component is low for the same. This in fact has led to tremendous rise in surface energy of GO as compared with UG and show absolute parity with the particle nature analysis data, reported in Table III. The average particle size of the commercially available expanded graphite is also compared in the same table (Table III). It shows that this filler is even more deagglomerated as it possesses still lower particle size than GO. As a consequence, expanded graphite has greater surface area as compared with GO.

X-ray diffraction and surface energy measurements

The X-ray diffractogram of the pristine graphite sample (UG) is displayed in Figure 2(a) along with that of the GO. The figure shows a very sharp diffraction peak at $2\theta = 28.6^\circ$ [Fig. 2(a)] for pristine graphite, which indicates high crystallinity and corresponds to the diffraction of the (002) plane.[39] The interplanar distance, d_{002}, was found to be 3.11 nm (Table IV). Oxidation via mixed acid treatment, forms graphite–acid intermediates, which comprises of carbon layers along with the polar groups–intercalated layers, stacked on top of one another. Heating this to sufficiently high temperature causes exfoliation of the graphite layers, forming vermicular or worm like shapes known as expanded graphite or thermo expanded graphite, already mentioned as GO. In GO, all peaks, including the characteristic peak are decreased in intensity from that of UG (Table IV) indicating the relative reduction in crystallinity after modification. The *d*-spacing for GO was calculated to be 3.16 nm, slightly greater than that of the pristine graphite sample. These observations corroborate the results obtained earlier by Uhl et al.[30] and indicate the transformation of UG in to a new crystalline form which may be lamellar, with slightly higher interlayer spacing. The following model nicely demonstrates this structural modification:

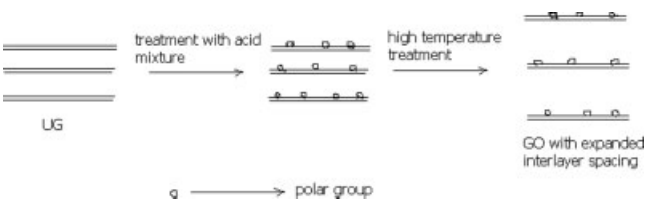

It may be mentioned here that the positions and the intensity of the diffraction peaks are subject to the nature of modification of the graphite samples. Figure 2(b) shows the X-ray diffractogram of EG. The crystallization peak for this system has been obtained at $2\theta = 26.1^\circ$ corresponding to an interlayer spacing (d_{002}) of 3.37 nm. This figure is slightly greater than that being obtained on modification of UG in the laboratory, although the crystallite size in both of these cases (GO and EG) are significantly lower than that of UG because of more deagglomerated structure. In addition, the expanded graphite, as is being observed previously through particle size analysis, possesses slightly lesser crystallite size than that of GO.

Analysis of EVA_{60}-graphite hybrid nanocomposites

FTIR, X-ray diffraction, and microscopy studies

Different analytical techniques described in the previous section have illustrated that the highly crystalline, naturally occurring graphite flakes (UG) has

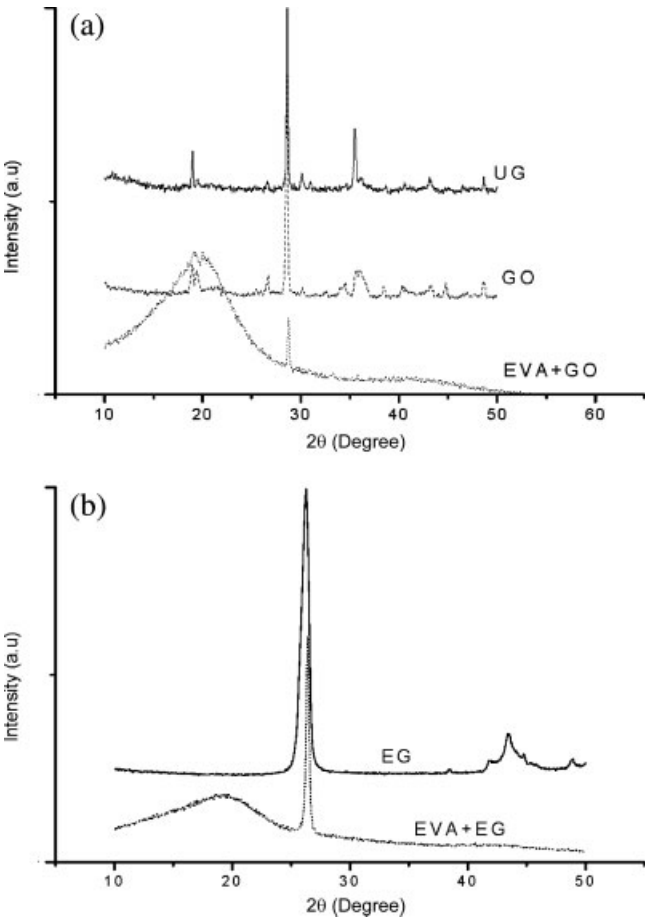

Figure 2 (a) X-ray diffractograms of the unmodified graphite, mixed acid modified graphite, and EVA_{60}-GO nanocomposite (2 phr GO concentration). (b) X-ray diffractograms of the commercially available expanded graphite along with its composite with EVA_{60} (4 phr filler concentration).

been transformed in to a polar, relatively amorphous graphite oxide (GO) with higher surface area. Figure 3 depicts the representative FTIR plots for virgin EVA (with 60% vinyl acetate content, denoted as EVA_{60}) and the EVA_{60}-GO hybrid nanocomposite with 2 wt % GO content, synthesized from solution intercalation process. There is virtually no difference in the nature of the spectra between these two systems except the appearance of the small band at 1565 cm^{-1}, which was originally present in the GO at 1665 cm^{-1} (Fig. 1). This indicates a stronger shift in the peak for C=C bond stretch (which was originally present in GO) towards lower wave number range, which indicates an increase in energy of the system. This may be due to stronger adsorption of the rubber over the GO surface or the stronger rubber-filler interaction. This would be further elaborated through swelling analysis of the samples, described in the later section.

The X-ray diffractograms of representative EVA-GO and EVA-EG samples are shown in Figure 2(a,b), respectively. For GO, the experiment has been carried out with 2 phr of the filler, whereas four parts of the filler has been used for the latter (as at these filler concentrations the respective composites show relatively better mechanical properties given in the later section). The broad peak at around $2\theta = 20^\circ$ corresponds to the amorphous halo. The principal crystalline peak in the modified graphite, in both the cases, does not shift to lower values, but the peak height reduces significantly.[39] Also, most of the small peaks, which are present in the case of GO disappear, indicating an increase in relative amorphousness in the composite (these small peaks are absent in the case of commercially available expanded graphite because of variation in treatment of the pristine graphite sample). Most importantly the crystallite size of the graphite does not change after the formation of the composite in either of these cases (Table IV). This virtually confirms the intercalated EVA-graphite structure formation using both GO and the expanded graphite in spite of different modification techniques adopted for these fillers.

Figure 4(a,b) demonstrates the AFM phase images of the GO and the UG filled EVA_{60} hybrid composites at 2 wt % filler concentrations, respectively. In the AFM figures, the harder phase i.e., the graphite is indicated in white, whereas the softer phase (rubber phase) is indicated in darker color. These figures very clearly distinguish between the nature of

TABLE IV
X-Ray Diffraction Data of Modified and Unmodified Graphites

	UG	GO	EG	EVA + 2 wt % GO	EVA + 4 wt % EG
Area of the characteristic peak of graphite	759	1,587	11,129	1,230	8,531
2θ (degree)	28.62	28.2	26.4	28.62	26.4
FWHM (degree)	0.17	0.24	0.63	0.20	0.38
Height of the characteristic peak of graphite (counts)	4,346	4,152	10,920	1,610	8,378
d (nm)	3.11	3.16	3.37	3.16	3.37
Crystallite size (nm)	8.42	5.97	2.06	5.97	2.06

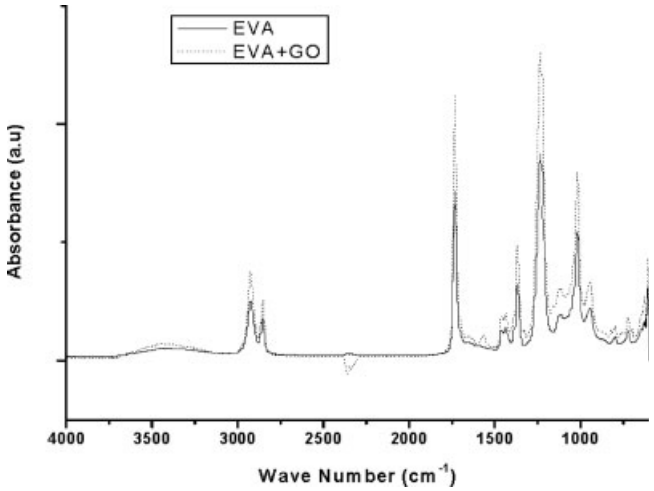

Figure 3 FTIR spectra of virgin EVA_{60} and the EVA_{60}-GO hybrid nanocomposite filled with 2 phr of GO.

dispersion of GO and UG within the EVA_{60} matrix [Fig. 4(a) for EVA_{60}-GO and Fig. 4(b) for EVA_{60}-UG]. GO is more uniformly distributed, and the thickness of the tactoids ranges from 10 to 40 nm [Fig. 4(a)], whereas the UG shows clear sign of agglomeration with average tactoid thickness of 50 nm or more in the rubber matrix, prepared under identical conditions. Furthermore, the GOs are more fribillar in appearance in Figure 4(a), which forms as a result of slightly more interlayer separation in GO where the rubber chains get access. This is further supported by the TEM image of EVA_{60}-GO hybrid nanocomposite (2 phr GO concentration) in Figure 4(c) where the finer distribution of graphite platelets in the rubber matrix is clearly seen (the clay phase is represented in black).

AFM phase image of the 4 phr EG filled EVA_{60} hybrid nanocomposite is elucidated in Figure 4(d). It can be observed from the figure that a network of graphite particles is formed in the rubber matrix leading to higher interaction between the matrix and the filler particles. The thickness of platelets are observed to be in the range of 20–30 nm and are almost comparable with that being obtained with GO [Fig. 4(a)]. However, there exists much finer layers (5–6 nm thick) inside the platelets, as observed in the magnified TEM image of the nanocomposite [Fig. 4(e)].

Dynamic mechanical thermal analysis and solvent swelling properties

Figure 5(a,b) represents the plots of dynamic storage modulus [Fig. 5(a), in log scale] and the loss tangent against temperature [Fig. 5(b)] for the hybrid nanocomposites. The experimental temperature ranges from -35 to $+20^{\circ}$C. In the glassy region, the moduli show steady increase from the virgin rubber with the concentration of GO up to 2 wt % beyond which these decrease. Similar trend exists in the transition region also. However, these moduli curves intercross each other at several points beyond this region and the moduli exhibit almost similar values [Fig. 5(a)]. On the other hand, the expanded graphite reinforced (4 wt %)-EVA_{60} nanocomposite exhibits quite a large value of storage modulus as compared with the other composites probably because of network morphology. Figure 5(b) illustrates the variation in tan δ values with temperature, demonstrating significant decrease in the peak height at 2 and 4 wt % of GO concentrations in the EVA_{60} from that of the virgin rubber. A steady shift in the tan δ_{max}, which indicates the T_g of the system, to higher temperature regions as a result of addition of GO is also noted. The expanded graphite reinforced system also shows reduction in peak height of tan δ curve. Moreover, the T_g is shifted only by 1°C from that of the virgin EVA_{60} sample. Table V denotes the moduli and tan δ values below, at and above the T_g regions, taken from Figure 5(a,b) for illustration. The T_g values are also included in the table. The increase in modulus on addition of GO is due to rubber-filler interactions, which is also evident from the FTIR spectra. Adsorption of the rubber chains over the GO surface causes partial immobilization of the rubber chains. This in turn decreases the vibrational amplitude at the glass transition and reduces the peak tan δ values. This is the case with up to 2 wt % of GO concentration where fillers are fibrillar and are more uniformly distributed. But at higher filler loading, say 4 wt %, some aggregation takes place, which actually reduces the available surface of the filler to interact with the rubber. This is reflected in the decrease of modulus for this system over that of the 2 wt % loaded $EVA_{60.}$ Furthermore, the peak area of the tan δ plots for the former is significantly lower than that of the latter, which indicates broader molecular weight distribution attained with finer particles and higher interaction with the GO at 2 wt % concentration. This is well supported by the results of the swelling study, reported in Table VI. More the volume fraction of the rubber entrapped in the swollen gel, higher is the swelling resistance. The nanocomposite filled with 2 wt % of GO shows the highest gel formation among all the systems (Table VI) and hence the maximum crosslink density (as the rubber-GO interaction points act as temporary fix points). The gel fraction values are low for 4 wt % GO loaded EVA_{60} composite as well as for 1 wt % UG loaded systems. In these cases, the less interactive filler surfaces or aggregation leave higher fraction of the rubber chains out of contact causing swelling. For 4 phr expanded graphite loaded sample, the maximum gel formation is recorded. This is

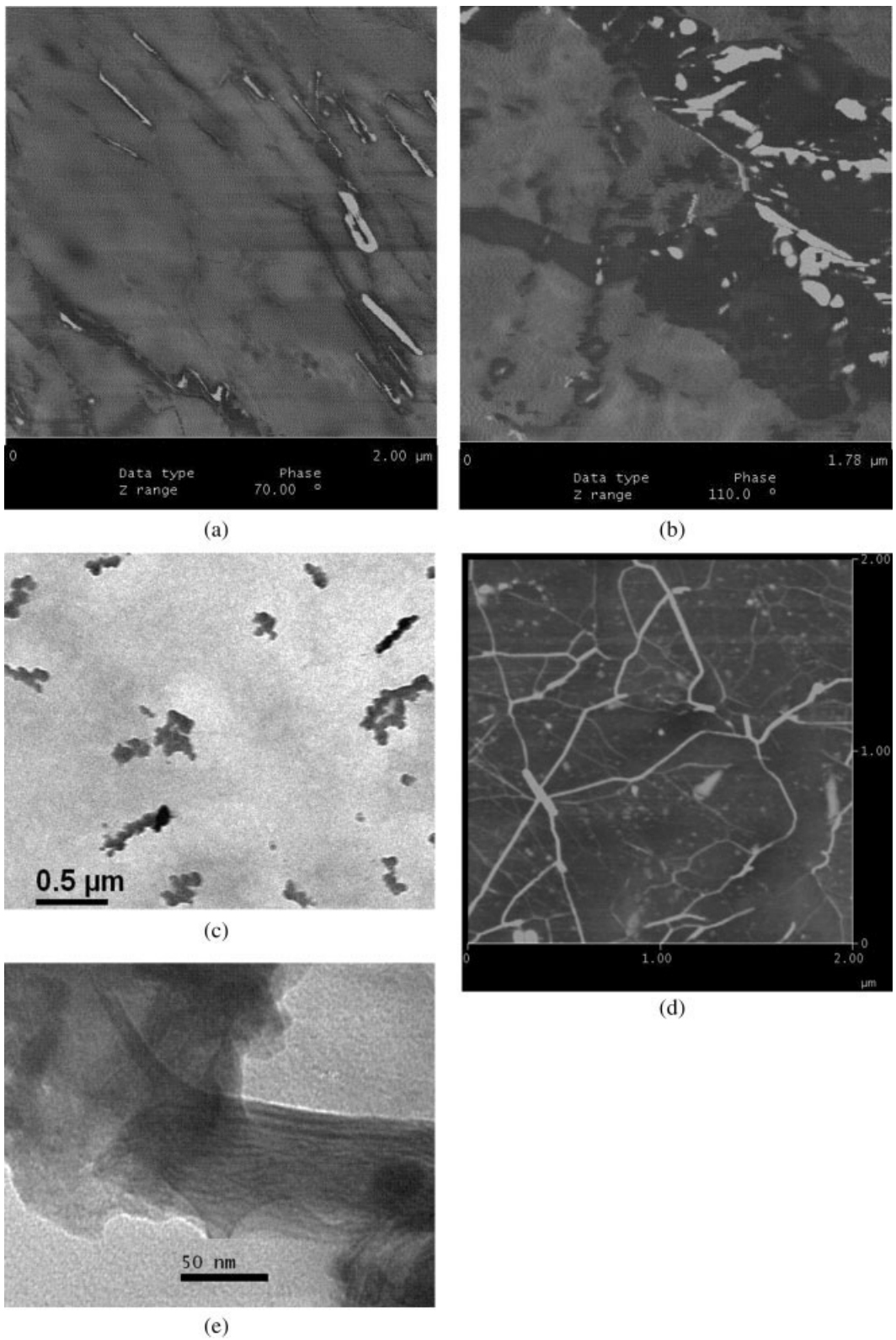

Figure 4 (a) AFM phase image of EVA_{60}-GO (2 phr). (b) AFM phase image of EVA_{60}-UG (2 phr). (c) TEM image of EVA_{60}-GO (2 phr). (d) AFM phase image of EVA_{60}-EG (4 phr). (e) TEM image of magnified graphite layer of EVA_{60}-EG (4 phr).

virtually due to higher surface area of the graphite and hence stronger interaction with the rubber matrix. These observations closely resemble the swelling phenomenon elucidated for nano silica and nano clay filled rubber systems reported from our laboratory.[40]

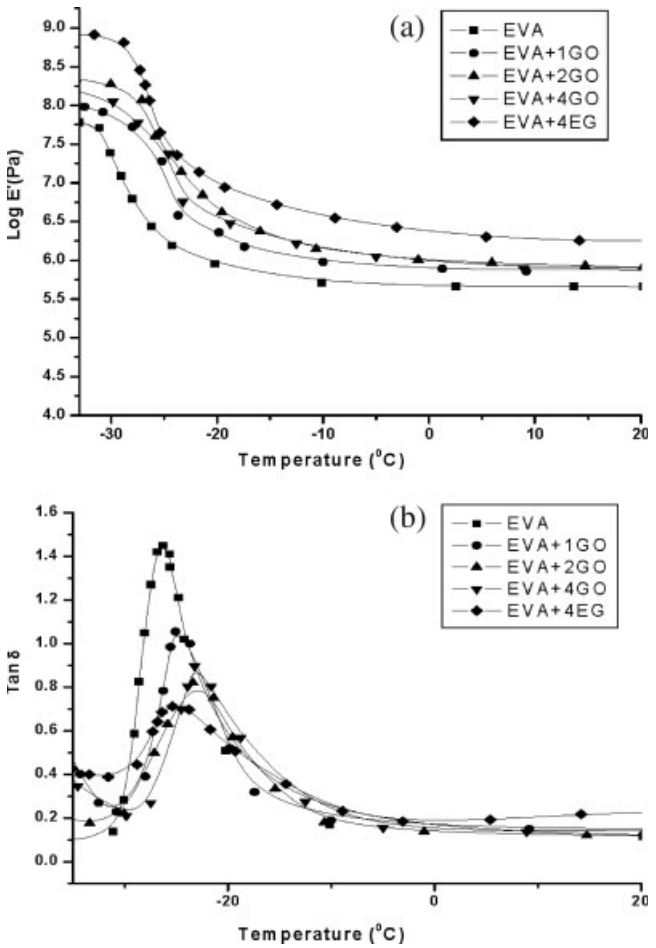

Figure 5 (a) Storage modulus versus temperature scans for the virgin EVA_{60} and EVA_{60}-GO hybrid composites at different GO concentrations, along with that of a representative EVA_{60}-EG (4 phr) nanocomposite. (b) Tan δ versus temperature scans for the virgin EVA_{60} and EVA_{60}-GO hybrid composites at different GO concentrations, along with that of representative EVA_{60}-EG (4 phr) nanocomposite.

Analysis of mechanical properties

Table VII reports in-detail mechanical properties of the cured EVA_{60}-graphite hybrid nanocomposites in terms of tensile modulus (at 50, 100, 200, and 300% elongations), tensile strength, and elongation at break (%) values. With increasing concentrations of the GO up to 2 phr, the strength and the modulus of EVA_{60}, increases because of effective rubber-filler interactions evident from the higher value of volume fraction of rubber. Maximum strength is obtained at 2 phr concentration, which is in line with the dynamic mechanical and swelling properties. At 4 phr GO concentration, these values are lower, indicating the effect of aggregation of the filler. A maximum of around 55% increment in the tensile strength with reference to the virgin EVA_{60} is attained. The lowering of strength beyond a critical value is due to the fact that there is aggregation of the nanographites and that higher surface area of the GO may also absorb some portion of the peroxide, thereby affecting the crosslinking reaction adversely. Although the tensile strength and modulus increase, the elongation at break does not decrease in the present system. This is possibly due to the slippage of the rubber chains over the fibrillar GO platelets, imparting some plasticizing effects within the system. In all the cases, this effect is evident but with different degrees (i.e., extent of increment varies), depending up on the state of dispersion of the GO. With UG, the mechanical properties are significantly lower than those obtained with similar doses of GO (Table VII) and even lower from those of the virgin EVA_{60} sample in the crosslinked nanocomposites. GO is comparatively more polar than UG, which facilitates better compatibility with the polar rubber-like EVA (polar–polar interaction) and hence promotes dispersion of the former. The UG phase, therefore, is more agglomerated [Fig. 4(b)] and is the point for stress concentrations and flaws, which cause lower strength and early failure of the hybrid composites. This behavior has been further confirmed by taking EVA having different vinyl acetate contents (not shown in the article). The expanded graphite filled EVA samples also exhibit a steady increase in mechanical properties with increasing filler content (Table VII). Up to 4 phr concentration studied, it shows an increasing trend. These nanocomposites show slightly higher modulus than that of the GO filled samples at similar GO concentrations, which may be due to network structure within the rubber matrix [Fig. 4(d)] and higher surface area of the filler (Table III). Contrastingly, the tensile strength values are slightly lower for these samples

TABLE V
Storage Modulus and Tan δ Values at Different Temperatures and T_g Values of the Hybrid Nanocomposites

		At T_g		At 0°C		At 20°C	
Samples	T_g (°C)	Log E' (Pa)	Tan δ	Log E' (Pa)	Tan δ	Log E' (Pa)	Tan δ
EVA	−26.5	6.45	1.45	5.70	0.17	5.66	0.12
EVA + 1GO	−24.8	7.21	1.17	5.98	0.17	5.85	0.14
EVA + 2GO	−22.8	7.02	0.77	6.07	0.14	5.91	0.15
EVA + 4GO	−23.0	7.40	0.79	6.04	0.15	5.71	0.12
EVA + 4EG	−25.4	7.72	0.71	6.38	0.19	6.24	0.22

TABLE VI
Solvent Swelling and Thermal Conductivity Data of EVA-Graphite Hybrid Composites

Sample	Volume fraction of rubber in swollen gel	Thermal conductivity from DSC (W/m/K/g)
EVA_{60}	0.071	0.23
EVA_{60} + 1GO	0.118	0.58
EVA_{60} + 2GO	0.126	0.60
EVA_{60}+4GO	0.112	0.42
EVA_{60} + 2UG	0.103	0.41
EVA_{60} + 4EG	0.138	–

than the corresponding GO filled samples, probably because of lesser technical compatibility of the filler with the polar rubber matrix (as the expanded graphite does not show the presence of any polar groups on its surface). Unlike GO filled samples, the elongation at break value decreases constantly on increasing the filler concentration. Higher concentration of the filler may have caused some aggregation in the bulk and thereby causes early failure and also minimizes the plasticization effect at the same time in the composite.

Studies on rheological behavior

Studies on the melt flow property of rubber nanocomposites are of particular interest, as it gives an impression about the processability of the system. Figure 6(a) describes the variation in apparent shear viscosity at different shear rates for the virgin EVA_{60} and EVA_{60} - GO hybrid nanocomposites. In all the cases, the shear viscosity drops nonlinearly on increasing the rate of shear, exhibiting the pseudoplastic nature of both the gum rubber and its nanocomposites. Moreover, addition of GO increases the viscosity of the system as noted from the figure [Fig. 6(a)]. Increase in viscosity of a polymeric system on addition of inorganic and organic fillers has been explained by Einstein[41] and Guth.[42] In the present investigation, the viscosity does increase on addition of GO, but not in an uniform fashion i.e., the viscosity values are almost similar for 1,2, and 4 wt % GO concentrations. This is probably due to the combined effect of finely dispersed fibrillar GO platelets, acting as dead rocks and allowing the slippage of the rubber chains (similar effect that delays the tensile failure of the hybrid nanocomposites) and some interaction between GO and the polymer. This result is quite similar to the earlier investigation on nanosilica and epoxy system where they displayed similar viscosity values for a range of shear rates.[43] Nitrile rubber-clay hybrid nanocomposites, reported from our laboratory[44] exhibited a completely different behavior. In those cases, the viscosity decreased with the concentration of clay platelets. Increasing viscous nature of the nanocomposites consequently improves the die swell behavior of these systems. The variations in die swell at different shear rates are displayed in Figure 6(b). All the systems have exhibited an overall increase in die swell on increasing the shear rate. Addition of small amount of GO decreases the die swell significantly. This is again explained on the basis of greater rubber-GO interaction in the previous case.

Thermal conductivity study

Figure 7 compares the heat flow curves of the virgin EVA and its representative hybrid nanocomposites from GO, determined by differential scanning calorimetry. The endotherm, as displayed by all the samples within the experimental temperature range of 140–165°C (25°C variation) is due to the intake of heat, which has been conducted through the sample. The experimental temperature range has been deliberately kept at such higher values to obtain substantial numerical values of the thermal conductivity, as the polymeric systems are common heat insulators. Thermal conductivity data (λ_1) calculated by employing Eq. (11) are reported in Table VI. The thermal conductivity increases on addition of graphite to EVA, which is quite expected. Interestingly,

TABLE VII
Tensile Properties of the Cured Nanocomposites

Sample	Tensile strength (MPa)	Elongation at break (%)	Modulus (MPa)			
			50%	100%	200%	300%
EVA_{60}	5.56 ± 0.20	335 ± 10	0.78 ± 0.05	1.21 ± 0.05	2.70 ± 0.10	5.35 ± 0.20
EVA_{60} + 1GO	7.10 ± 0.20	330 ± 10	0.78 ± 0.05	1.24 ± 0.05	2.75 ± 0.10	5.66 ± 0.10
EVA_{60} + 2GO	8.63 ± 0.25	340 ± 10	0.80 ± 0.05	1.27 ± 0.05	2.80 ± 0.10	6.38 ± 0.15
EVA_{60} + 4GO	6.14 ± 0.25	330 ± 10	0.79 ± 0.05	1.19 ± 0.05	2.34 ± 0.10	4.75 ± 0.15
EVA_{60} + 1UG	5.18 ± 0.20	320 ± 10	0.74 ± 0.05	1.13 ± 0.05	2.20 ± 0.10	4.01 ± 0.10
EVA_{60} + 2UG	4.83 ± 0.20	310 ± 10	0.68 ± 0.05	0.98 ± 0.05	1.82 ± 0.10	3.55 ± 0.10
EVA_{60} + 4UG	4.59 ± 0.20	310 ± 10	0.66 ± 0.05	0.94 ± 0.05	1.68 ± 0.10	3.20 ± 0.10
EVA_{60} + 1EG	6.03 ± 0.20	345 ± 10	0.86 ± 0.05	1.28 ± 0.05	2.92 ± 0.10	5.23 ± 0.15
EVA_{60} + 2EG	6.58 ± 0.20	330 ± 10	0.95 ± 0.05	1.54 ± 0.05	3.44 ± 0.10	6.24 ± 0.15
EVA_{60} + 4EG	7.51 ± 0.20	320 ± 10	1.26 ± 0.05	2.05 ± 0.05	4.14 ± 0.10	7.20 ± 0.20

TABLE VIII
TGA and DTG Data of the Hybrid Composites

Samples	Onset of degradation (°C) (from TG)	Temperature of maximum rate of degradation(°C) (from DTG)	Residue at 600°C (%) (from TG)
EVA_{60}	250	480	0.16
EVA_{60} + 1GO	254	482, 494	0.96
EVA_{60} + 2GO	257	480, 498	2.10
EVA_{60} + 4GO	252	480	4.16
EVA_{60} + 4EG	270	497	4.29

the λ_1 value reaches maxima at 2 phr (160% of increase) of GO concentration, whereas it is low for both 1 and 4 phr. Finer dispersion in fibrilar form of GO at 2 phr concentration enhances interaction with EVA and favors better heat transfer of the nanocomposites. With 1 phr of GO concentration, this effect probably has not been optimized because of smaller concentration of the filler, while at 4 phr, aggregation of the filler decreases the rubber-filler interaction and demonstrates adverse effect on the thermal conductivity of the hybrid composites.

Thermoxidative degradation

Figure 8(a,b) demonstrates the TGA and DTG plots of the virgin EVA and its hybrid nanocomposites, carried out under oxygen. Thermal degradation studies under oxygen furnish near-practical data of the composites and express the oxidative stability under drastic external conditions. Virgin EVA_{60} shows two-stage degradation probably because of the oxidation of side chains and main chains, respectively. Addition of GO to EVA_{60} does not change the nature of degradation as observed from the TGA plots in Figure 8(a). The temperatures corresponding to the onset of degradation (Ti) of these samples are reported in Table VIII. There is a slight shift in T_i towards higher temperature for the hybrid composites from that of the virgin EVA_{60}. The T_i for the hybrid composites as reported in Table VIII reveals the highest value at 2 phr of GO concentration and has complemented the thermal conductivity data (enlisted in Table VI) very nicely. Finer dispersion of GO could act as ''efficient heat sinks,'' which consumes more heat than the matrix and does not allow the accumulation of heat within the latter and thereby prevents oxidation at the early stages of degradation. The rate of degradation in the second phase, which is observed in the principal degradation range (from 450 to 550°C) of EVA_{60} is significantly improved with the incorporation of GO in the rubber matrix [Fig. 8(b), the DTG plots] in comparison to the first phase of degradation (from 300 to 400°C). The peak heights of the DTG plots at the higher temperature range (second phase degradation) is dropped noticeably at 2 phr GO concentration, while for other GO concentrations, this drop is slightly less. This shows a reduction in the maximum rate of degredation with the addition of GO. Also, the peak degradation temperature is shifted to higher values for 1 and 2 phr of GO concentrations. With 4 phr of GO, this value is not much higher than that of the neat rubber sample. The residue obtained at the end of the degradation increases with the increase in GO concentration as usual (Table VIII). These values are slightly less for the hybrid composites when these are compared with the theoretically calculated values. This may be due to slight oxidation loss of the GO at higher temperatures. The expanded graphite-EVA_{60} nanocomposite exhibits a tremendous increase in thermal stability when compared with the virgin EVA_{60} and also with GO filled EVA_{60} nanocomposites. With 4 wt % of expanded graphite, the onset of degredation showed a 20°C shift towards higher temperature region, whereas

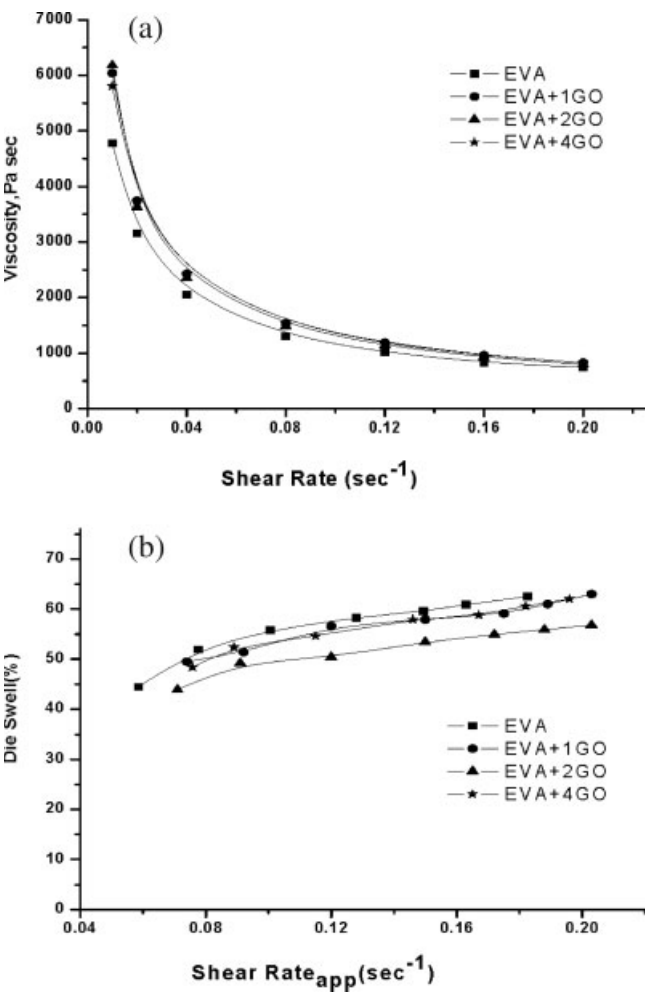

Figure 6 (a) Apparent shear viscosity versus shear rate plots for neat and GO loaded EVA_{60} nanocomposites. (b) Die-swell versus shear rate plots for neat and GO loaded EVA_{60} nanocomposites.

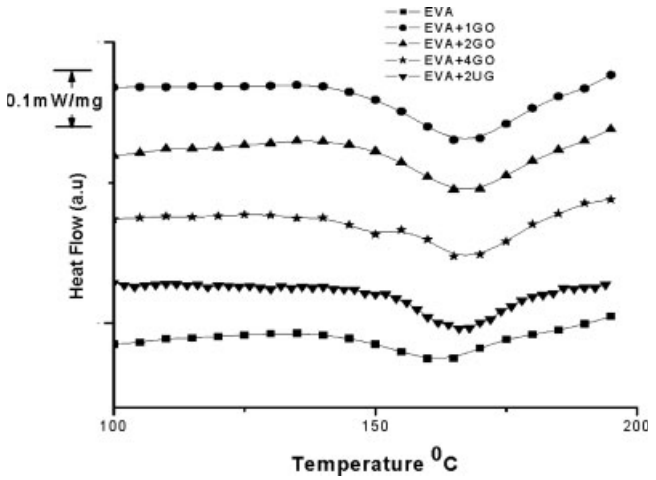

Figure 7 DSC scans for virgin EVA_{60} and its hybrid composites at different GO concentrations within the temperature range of 140–165°C.

the temperature of maximum rate of degradation exhibits more than 15°C shift. This may be due to network structure of expanded graphite within the matrix and also better interaction with rubber.

CONCLUSIONS

Thorough investigation on the modification of naturally occurring graphite and characterization of the novel EVA_{60}-graphite hybrid composites have been reported extensively in this article. The elaborate discussion on the experimental findings ultimately leads to the following conclusions:

1. Treatment with mixed acid (H_2SO_4 and HNO_3) and subsequent heating at higher temperature causes most effective oxidation of the graphite as compared with other reagents. This has been inferred from FTIR spectra and size of the particles. XRD study on this modified graphite has illustrated slight increase in the interlayer spacing in the graphene layers from that of the unmodified sample. The sample is also little deagglomerated and possesses almost double the surface energy than that of the virgin graphite. The commercially available expanded graphite, on the other hand, does not possess any polar groups on its surface but are slightly more deagglomerated (possess smaller particle size and higher average surface area) with higher intergallery distance compared with the acid treated GO.
2. At similar concentration, the modified graphite shows better dispersion in the EVA matrix having 60% vinyl acetate content (than the unmodified sample), as illustrated from the AFM (phase image) and TEM studies. The expanded graphite also shows finer dispersion with some network formation. In both the cases the intercalated nanocomposites have been obtained. The UG has produced more aggregated filler morphology within the rubber matrix.
3. Better dispersion of the modified graphite results in higher dynamic modulus of the hybrid composites, the optimum being achieved with 2 phr of GO, beyond which the properties show lesser improvement because of the aggregation of the filler. The loss tangent curve shows maximum widening and lowering of the peak height at this concentration. The glass-rubber transition has also shifted to higher temperature illustrating more restricted chain movements in the rubber matrix. Representative expanded graphite-EVA nanocomposite (four parts of filler concentration) also exhibits higher modulus and higher glass-rubber transition temperature than those of the virgin rubber sample. The rubber-filler interaction at different level of filler con-

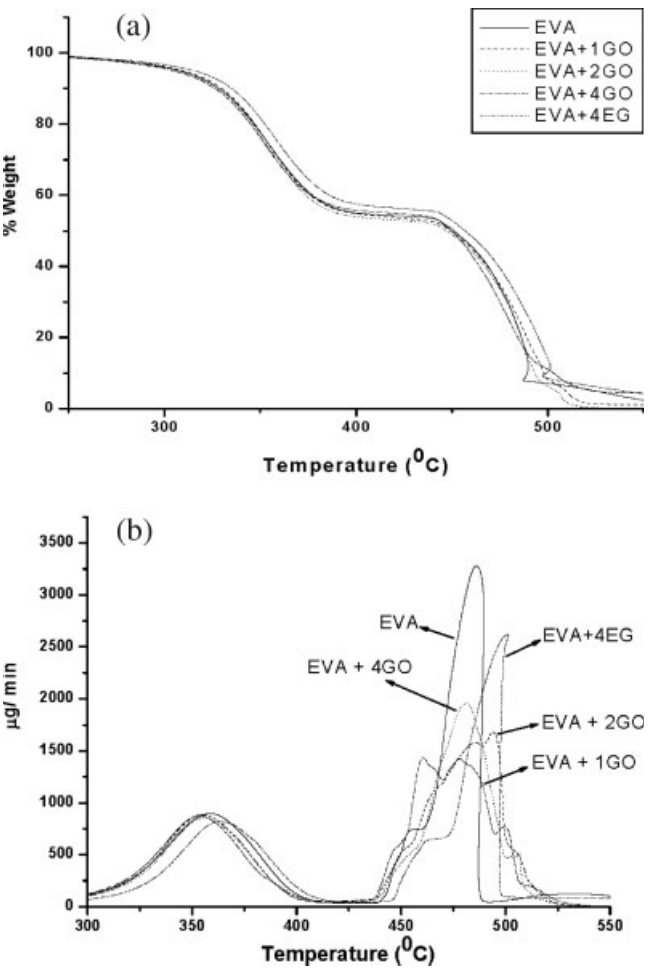

Figure 8 Thermo oxidative degradation plots for EVA_{60} and its GO loaded hybrid composites along with that of EVA_{60}-EG (4 wt %) nanocomposite: (a) TGA and (b) DTG.

centrations receives further confirmation from the solvent swelling study.

4. The tensile properties of the hybrid composites are superior to those of the virgin rubber samples, showing the reinforcing action of the modified graphite. Again, the maximum reinforcing action has been displayed by the sample having two parts of GO concentration due to highest rubber-filler interaction. The reinforcing action decreases at higher filler concentration due to aggregation. These effects have been further demonstrated in the rheological studies of the hybrid composites. The expanded graphite on the other hand displays a gradually increasing trend in tensile strength and modulus of the composite up to four parts loading. The modulus values at a particular filler concentration are higher for the commercial filler which may be due to relatively more rubber intercalation and higher surface area.
5. All the EVA_{60}-GO hybrid composites have higher thermal conductivity as illustrated from the DSC experiment. They are also thermally more stable under oxygen, than the virgin rubber sample. Because of better dispersion of the modified graphite at 2 wt % concentration, all these properties show maxima at this composition, once again illustrating the effect of better rubber-filler interaction.

The thank Mr. Anirban Ganguly and Ms. Madhuchanda Maiti for AFM measurements.

References

1. Karger-Kocsis, J. Polym Eng Sci 2004, 44, 1083.
2. Ray, S. S.; Okamoto, M. Prog Polym Sci 2003, 28, 1539.
3. Pattanayak, A.; Jana, S. C. Polym Eng Sci 2005, 45, 1532.
4. Donnet, J. B. Compos Sci Technol 2003, 63, 1085.
5. Bandyopadhyay, A.; De Sarkar, M.; Bhowmick, A. K. J Mater Sci 2005, 40, 5233.
6. Butterworth, M. D.; Corradi, R.; Johal, J.; Lascelles, S. F.; Maeda, S.; Armes, S. P. J Colloid Interface Sci 2005, 174, 510.
7. Feng, Y.; Ria, Y.; Gordon, N. L. J Fire Sci 2005, 23, 209.
8. Cynthia, M. A.; Krishnamoorti, R. Polymer 2005, 46, 8796.
9. Bhattacharyya, A. R.; Sreekumar, T. V.; Liu, T.; Kumar, S.; Ericson, L. M.; Hauge, R. H.; Smalley, R. E. Polymer 2003, 44, 2373.
10. Park, J. H.; Jana, S. C. Macromolecules 2003, 36, 2758.
11. Cser, F.; Bhattacharya, S. N. J Appl Polym Sci 2003, 90, 3026.
12. Sadhu, S.; Bhowmick, A. K. Rubber Chem Technol 2005, 78, 321.
13. Maity, M.; Sadhu, S.; Bhowmick, A. K. J Polym Sci Part B: Polym Phys 2004, 42, 4489.
14. Zhang, W.; Chen, D.; Zhao, Q.; Fang, Y. K. Polymer 2003, 44, 7953.
15. Altintzi, C. I.; Anastasiadis, S. H.; Giannelis, E. P.; Pitsikalis, M.; Hadjichristidis, N. Polymer 2005, 46, 12440.
16. Kader, M. A.; Kim, K.; Lee, Y. S.; Nah, C. J Mater Sci 2006, 41, 7341.
17. Sarazin, F. P.; Ton-That, M. T.; Bureau, M. N.; Denault, J. Polymer 2005, 46, 11624.
18. Hedicke, K.; Wittich, H.; Mehler, C.; Gruber, F.; Altstädt, V. Compos Sci Technol 2006, 66, 571.
19. Zhang, J.; Jiang, D. D.; Wilkie, C. A. Polym Degrad Stab 2006, 91, 298.
20. Wang, S.; Hu, Y.; Zhongkai, Q.; Wang, Z.; Chen, Z.; Fan, W. Mater Lett 2003, 57, 2675.
21. Bandyopadhyay, A.; De Sarkar, M.; Bhowmick, A. K. J Mater Sci 2005, 40, 53.
22. Maeda, S.; Gill, M.; Armes, S. P.; Fletcher, I. W. Langmuir 1995, 11, 1899.
23. Patel, S.; Bandyopadhyay, A.; Vijayabaskar, V.; Bhowmick, A. K. Polymer 2005, 46, 8079.
24. Chow, P. Y.; Gan, L. M. J Nanosci Nanotechnol 2004, 4, 197.
25. Dresselhaus, M. S. Graphite Fibers and Filaments; Springer-Verlag: London, 1988.
26. Ping, W. W.; Yuan, P. C. Polym Eng Sci 2004, 44, 12.
27. Inagaki, M.; Tashiro, R.; Washino, Y.; Toyoda, M. J Phys Chem Solids 2004, 65, 133.
28. Matsuo, Y.; Tahara, K.; Sugie, Y. Carbon 1997, 35, 113.
29. Xiao, M.; Sun, L.; Liu, J.; Li, Y.; Gong, K. Polymer 2002, 43, 2245.
30. Uhl, F. M.; Lamelas, F. J.; Wilkie, C. A. 220th ACS National Meeting, Washington, DC, August 20–24, 2000.
31. Bhowmick, A. K.; Stephens, H. L. Handbook of Elastomers; Marcel Dekker: New York, 2001.
32. Chen, G.; Wu, C.; Weng, W.; Wu, D.; Yan, W. Polymer 2003, 44, 1781.
33. Gopakumar, T. G. Polym Eng Sci 2004, 44, 1162.
34. Basiuk, E. V.; Pelaez, M.; Lee, P. I.; Basiuk, V. A. Nano Lett 2004, 4, 863.
35. Cullity, B. D. Elements of X-Ray Diffraction; Addison Wesley: Reading, MA, 1978.
36. Alexander, L. E. X-Ray Diffraction Methods in Polymer Science; Wiley: New York, 1969.
37. Shanmugharaj, A. M.; Sabharwal, S.; Majali, A. B.; Tikku, V. K.; Bhowmick, A. K. J Mater Sci 2002, 37, 2781.
38. Sadhu, S.; Bhowmick, A. K. J Polym Sci Part B: Polym Phys 2004, 42, 1573.
39. Chen, G. H.; Wu, D. J.; Weng, W. G.; Yan, W. L. J Appl Polym Sci 2001, 82, 2506.
40. Bandyopadhyay, A.; De Sarkar, M.; Bhowmick, A. K. J Polym Sci Part B: Polym Phys 2005, 43, 2399.
41. Einstein, A. Annalen der Physik (Weinheim, Germany) 1905, 17, 549.
42. Guth, F. J Appl Phys 1945, 16, 20.
43. Bandopadhyay, A.; De Sarkar, M.; Bhowmick, A. K. Rubber Chem Technol 2005, 78, 806.
44. Sadhu, S.; Bhowmick, A. K. J Polym Sci Part B: Polym Phys 2005, 43, 1854.